Effect of longitudinal interfacial defects on fracture energy variation in DCB bonded specimens

Mahfoudh TALEB ALI[1], Zaineb JEBRI[2], Julien JUMEL[1]

[1]University of Bordeaux, I2M, UMR 5295, F-33400 Talence, France.

[2]University of Bordeaux, IMS, UMR 5218, F-33400 Talence, France.

Corresponding author: talebali.mahfoudh@gmail.com

Abstract:

The primary aim of this investigation is to develop an analytical technique that can accurately estimate the fracture energy at the crack front while accounting for the localized interface properties. To achieve this goal, the study employs Double Cantilever Beam (DCB) specimens made of Aluminium alloys that have been chemically treated, as well as Titanium alloys that have been Laser texturized. Additionally, longitudinal defects are introduced within the bond line, specifically at the interface between the adhesive and adherents, with a parallel orientation to the crack direction. Initially, the investigation involved the characterization of bare surfaces, independent of their adhesive strength. Subsequently, Double Cantilever Beam (DCB) tests were conducted on specimens that had defects of various widths in the bonded region. The results obtained from these experiments confirmed the accuracy of the analytical estimations. It has been explained too that adhesive stiffness has a major role while mixing local fracture energies at crack front. Additionally, using a damage model, the deformation of the crack front was numerically observed and verified by capturing crack front shape while DCB testing. An interpretation was provided to explain the findings.

Keywords:

DCB testing, Laser texturizing, Moment based approach, crack front shape, fracture energy, longitudinal defects, mechanical resistance, crack propagation, adhesive stiffness, analytical approach.

1. Introduction

Adhesive bonding is extensively used in numerous commercial programs due to its advantages, which includes weight loss, improved aesthetics, and extended joint power. However, the first-class of the adhesive joint is a crucial aspect that affects the durability and longevity of the bonded assembly. The defects, that can purpose premature failure of the shape, are typically caused by negative floor treatment leading to a discontinuity within the bond line or the inclusion of heterogeneities in the course of bonding or pre-bonding. Adhesive defects occur whilst there's inadequate adhesion between the adhesive and the substrate being bonded. This may be resulting from a selection of things, along with infection, insufficient surface training, unsuitable curing of the adhesive, or the usage of an adhesive that isn't always appropriate for the precise software. Adhesive defects can bring about a vulnerable bond this is at risk of failure, or in a few instances, entire separation of the bonded surfaces.

While numerous studies have been carried out on transverse defects in bonded assemblies as in (Budzik & Jensen, 2016), (Karachalios, Adams, & DaSilva, 2013), (Tadepalli, Turner, & Thompson, 2008) et (Ranade S. , 2014), (Jumel, 2017), (Jorgensen & Budzik, 2017), (TalebAli, Jumel, & Shanahan, 2018), (Cuminatto, Parry, & Braccini, 2015), (Taleb Ali, 2018), longitudinal defects have not been studied in as much detail and researchers doesn’t give much interest in these types of defects. Longitudinal defects can include cracks, voids, delamination, or other types of irregularities that run parallel to the direction of the bond line. These defects have been found to significantly impact the mechanical properties and structural integrity of

bonded assemblies, yet further research is needed to fully understand their effects and develop effective mitigation strategies. Some studies have been carried out in this subject. (Budzik, Jumel, & Shanahan, 2013) investigated the fracture of adhesive joints with variable interfacial properties using polycarbonate plates with weak or strong interfaces bonded to aluminium blocks using an epoxy adhesive. The study found that global elastic fracture energy is not linearly dependent on the weak/strong interface mixture as suggested by classical "elastic" rules of mixtures. The existence of a crossover zone, where strong and weak parts of the interface interact through the continuity of the adhesive film, is suspected to be at the heart of the problem. The study suggests an appropriate empirical model inspired by rheological models and highlights the need for more complex studies to examine the interaction between strong and weak zones.

The evolution of the energy release rate as a function of the high/low adhesion fraction is a topic of interest for many research teams. Some, like (Budzik, Jumel, & Shanahan, 2013)and (Litteken & Dauskardt, 2003), have observed a non-linear variation of the fracture energy as a function of the surface fraction of high/low adhesion. In contrast, (Ranade, et al., 2018) and (Chan, Ahn, & Crosby, 2007) found a linear variation.

Interfacial complex defects within adhesive joint are a mixture of transverse and longitudinal defects. The present study is a continuation of the paper (TalebAli, Jumel, & Shanahan, 2018)where the effect of transverse adhesion defects has been determined so we can deal later with complex defects.

2. Materials and methods

In this study, double cantilever beam specimens were used to test interface resistance since they allow crack propagation according to mode I failure. Aluminium Alloy 7075-T6 and Titanium

alloy Ti6A14V were considered to realise Double Cantilever Beam specimens. The table 1 and figure 1 contains all substrates information.

Specimens manufacturing parameters and conditions are the same as used in (TalebAli, Jumel, & Shanahan, 2018)and (Taleb Ali, 2018). The DCB specimen is composed of 2 essential parts. The first one is a non-bonded area which represents a pre-crack for crack initiation. The non-bonded length is noted a_0, see figure 1.

Table 1: Specimens dimensions

	Aluminium Alloy 7075-T6	Titanium Alloy Ti6A14V
Width w (mm)	25	25
Thickness t (mm)	5	1.6
Length L (mm)	200	200

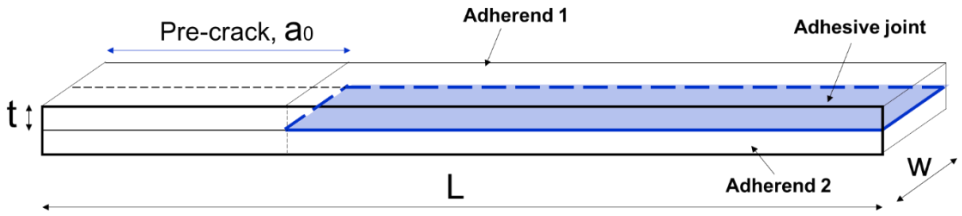

Figure 1: Substrate sketch and configuration.

The nominal state of interface adhesion is achieved by chemical etching on Aluminium slabs and Laser surface treatment for Titanium slabs. Etching protocol of Aluminium slabs were achieved as in (Taleb Ali, 2018) leading to a surface state ready for bonding. Within the chemical etching process, a NaOH based solution was used for etching and a P2 solution was used for anodising. Concerning Titanium substrates, a nanosecond laser treatment at ambient

temperature was used. Laser average power, scanning speed and cross-hatch pitch are respectively 4W, 250mm/s and 10µm (see figure 2). After Laser treatment, substrates were cleaned in deionized water ultrasonic bath and then dried with hot air. This treatment led to a mechanically active surface by creating a significant roughness which improves mechanical anchoring of the adhesive (Loumena, Cherif, Taleb Ali, & Kling, 2017), see figure 3.

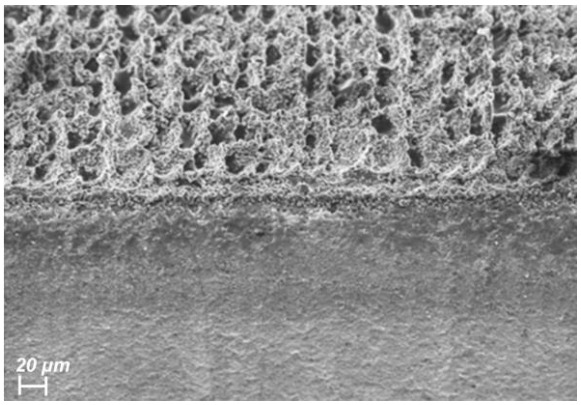

Figure 2: Surface aspect after laser treatment on titanium alloy substrates.

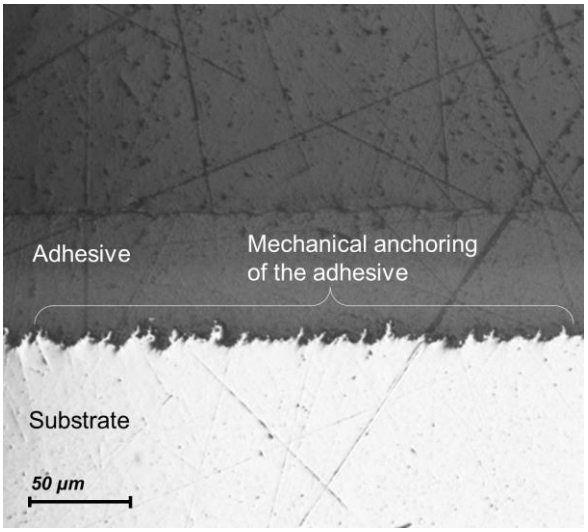

Figure 3: anchoring of the adhesive inside substrate roughness

Non-supported structural adhesive film (Scotch-Weld, 2009) was used to bond both aluminium substrates and titanium substrates and to guarantee a constant thickness of the adhesive all along the specimen and to delimit the adhesive while curing, a 0.1 mm PTFE sticker film was stuck to the border as shown in figure 4.

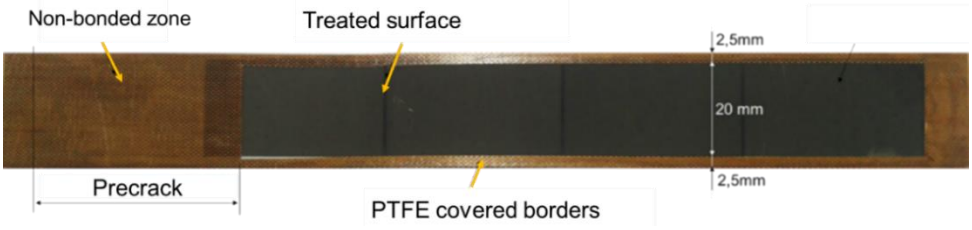

Figure 4: Configuration of an adherent surface

The experimental campaign includes tests on both Aluminium alloy and Titanium alloy specimens. The configurations done on Aluminium alloys DCB specimens are as shown in figure 5 and only one surface was artificially contaminated by PTFE depositing. In figure 5, “d” is the width of the central longitudinal region which has “bad” adhesion. Whereas the rest has “good” adhesion.

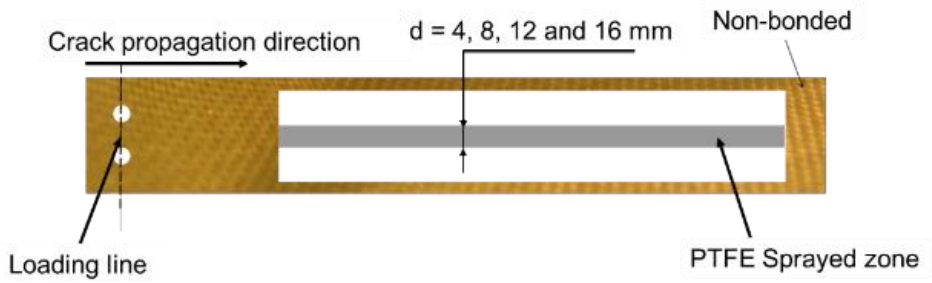

Figure 5: configuration chosen for aluminium alloy substrates.

For Titanium alloys, as can be seen in figure 6, the configuration chosen for this test is a continuous variation of the well-treated surface which is leading to a “good” adhesion. The triangle form in this case allows a continuous variation of the parameter “d” which is the width of the “good” adhesion region. The same case as for Aluminium alloys, only one surface has undergone a surface treatment variation. The coloured zones in the figure below represents the laser treated areas. The table 2 presents the substrates combination to form DCB specimens needed for the experiment.

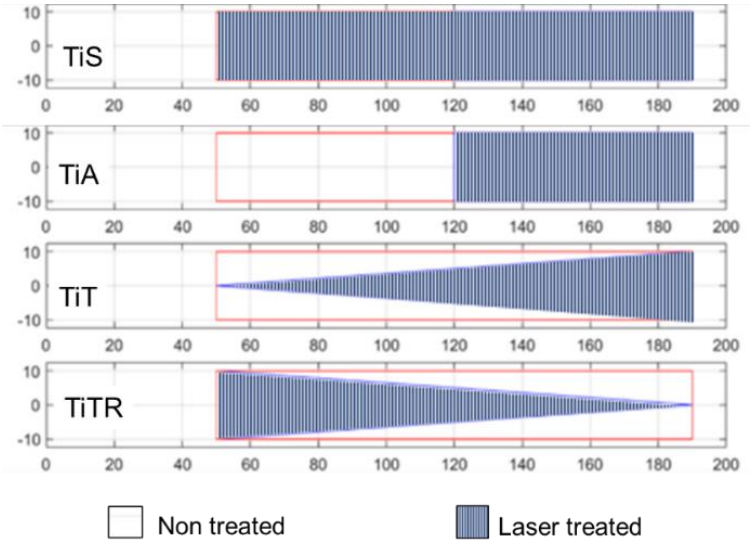

Figure 6: Titanium alloy specimen

Table 2: DCB specimen's combinations

Combination	TiS + TiS	TiS + TiA	TiT + TiS	TiTR + TiS

A speckle was deposited on specimen's sides to serve for Digital Image Correlation (DIC) and two end blocks were finally screwed to the specimens used for load application. The test set up shown if figure 7 also includes two inclinometers. They serve to measure the inclination angle used to compute the fracture energy of the bonded joints.

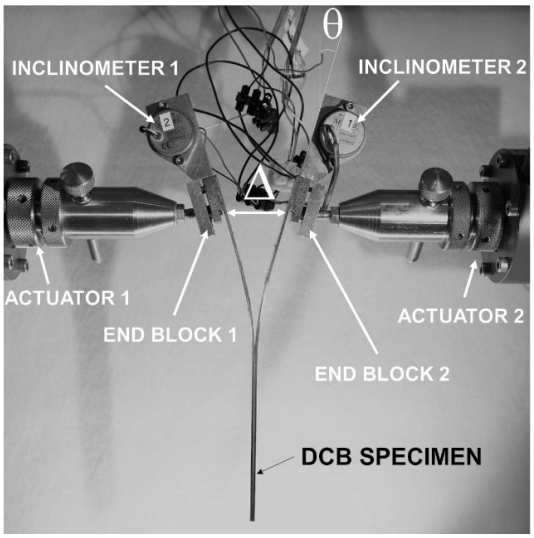

Figure 7: Loading set up of Aluminium and Titanium alloy DCB specimens with inclinometers.

The specimen is loaded with a dual actuator system composed of two EZ001 Zwick electromechanical actuators. The actuators are placed horizontally, opposite to each other. Once attached with the end block to the machine, the specimen is vertical. A constant 1mm/min displacement rate is set on both actuators resulting in ≈2mm/min specimen opening rate.

Thanks to the symmetry of the dual actuator configuration, the bond line remains at the same vertical position during the experiment, facilitating video monitoring using a Canon Eos 70D digital camera. During the test, the force applied on each adherent is monitored with two **1kN** load cells.

During DCB tests on Aluminium alloy specimens, a penetrant liquid has been injected in the crack front to mark the shape and distinguish its variation from a bad and good adhesion area.

The next paragraph shows the analytical development that highlights the propagation of a crack inside an adhesively bonded joint of DCB specimen's considering longitudinal defects.

3. Analytical model of fracture energy evolution at crack front:

As a reminder and as has been done in multiple reviews, the apparent crack propagation length noted “a” inside a DCB specimen is expressed as below:

$$a = \sqrt[3]{\frac{3EI}{2}\frac{\Delta}{P}} \tag{1}$$

With

E: Young’s Modulus of the adherent material.

I: Quadratic moment which is equal to: $wt^3/12$.

P: is the measured load.

And Δ is the measured opening (separation between the adherents in the loading line).

The energy necessary for the fracture of the DCB specimen bonded joint, is expressed by equation (2):

$$Gc = \frac{a^2P^2}{wEI} \tag{2}$$

And finally, the force necessary for crack propagation in relation with the specimen opening and crack length is expressed as in equation (3):

$$P = (wG_c)^{3/4}\left(\frac{9}{4}EI\right)^{1/4}\frac{1}{\sqrt{\Delta}} \tag{3}$$

For both specimens, Aluminium and Titanium alloys, the fraction of the “strong” region is denoted “f_s” and the “weak” one is denoted “f_w”. They are calculated as below:

$$f_s = \frac{w - d}{w} \tag{4}$$

And

$$f_w = \frac{d}{w} \tag{5}$$

We introduce too Gcw and Gcs as the critical fracture energy of a “weak” and a “strong” interface respectively such as:

$$Gc = (1 - f_w)\, Gc_s + f_w\, Gc_w \tag{6}$$

The opening force, P, applied to separate adherents must be balanced by the cohesive forces in the substrates at the crack front which can be decomposed as follows:

$$P = P_s + P_w \tag{7}$$

Where Ps is the force applied in the zone of strong adhesion (cohesive failure) and Pw represents the force applied in the weak zone. Then, the opening can be written using Gcw and Gcs as:

$$P = \left(\frac{Et^3}{27\Delta^2}\right)^{1/4} \left[w_s\, {Gc_s}^{3/4} + d\, {Gc_w}^{3/4}\right] \tag{8}$$

So, the fracture energy Gc can be expressed as follows:

$$Gc = \frac{3P^{4/3}}{t}\left(\frac{\Delta^2}{Ew^4}\right)^{1/3} \quad (9)$$

By rearranging the last equation, Gc can be written also as:

$$Gc = Gc_s\left[r^{\frac{3}{4}} + f_s\left(1 - r^{\frac{3}{4}}\right)\right]^{\frac{4}{3}} \quad (10)$$

With $\boldsymbol{r = \frac{Gc_w}{Gc_s}}$

A second theory suggests that decohesion propagation is primarily controlled by the bending moment applied to the crack front rather than by the shear force. The flow of moment causing the propagation is therefore:

$$M = \frac{\sqrt{EIwGc}}{w} \quad (11)$$

The bending moment at the crack front in both “weak” and “strong” regions is expressed as:

$$M_{tot} = \frac{\sqrt{EIdGc^w}}{w} + \frac{\sqrt{EI(w-d)Gc^s}}{w} \quad (12)$$

So the fracture energy can be written as:

$$Gc = Gc^s\left(f_w\sqrt{r} + (1 - f_w)\right)^2 \quad (13)$$

4. Tests and results

4.1.Characterization of homogenous interfaces:

To commence this study, we characterize the homogeneous "weak" and "strong" interfaces in DCB specimens made of both Aluminium and Titanium alloys, as demonstrated in Figure 8. The analytical estimate corresponds to equation 3.

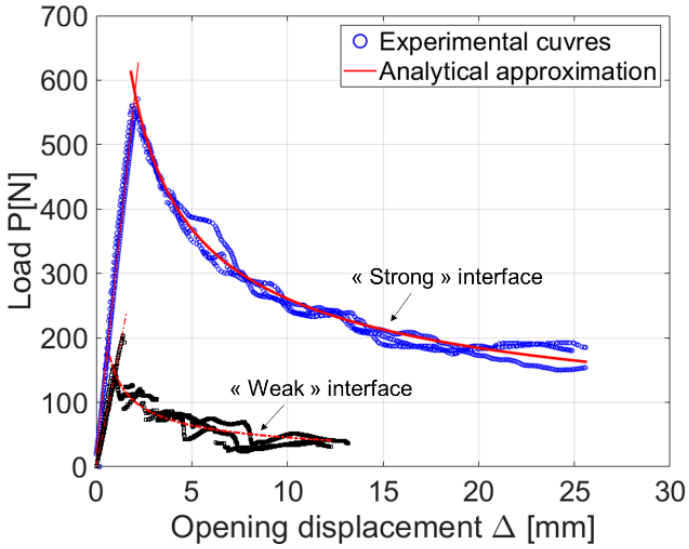

Figure 8: Mechanical behaviour of strong and weak interfaces

of Aluminium DCB Specimens

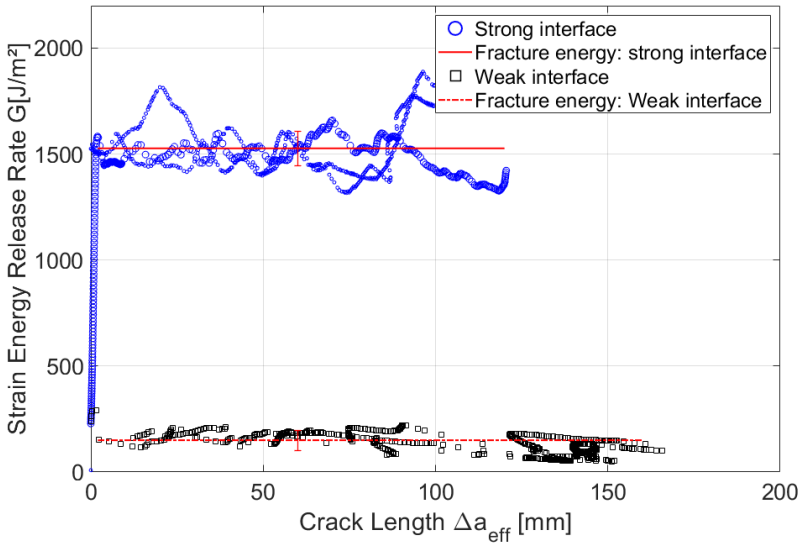

Figure 9: Evolution of the strain energy release rate.

In Figure 9, the progression of the energy strain rate with respect to the crack length is displayed in one of the tested aluminum alloy specimens. The flat portion of the curve indicates the fracture energy at the crack front. The strong and weak interfaces require approximately 1500 J/m² and 150 J/m², respectively, to initiate cracking. Figure 10 demonstrates the characterization of homogeneous interfaces in DCB specimens made of titanium alloy. (TiS+TiS) and

(TiA+TiS) specimens were tested, which consist of two strong interfaces and a weak interface with a half strong interface in both adherents, respectively.

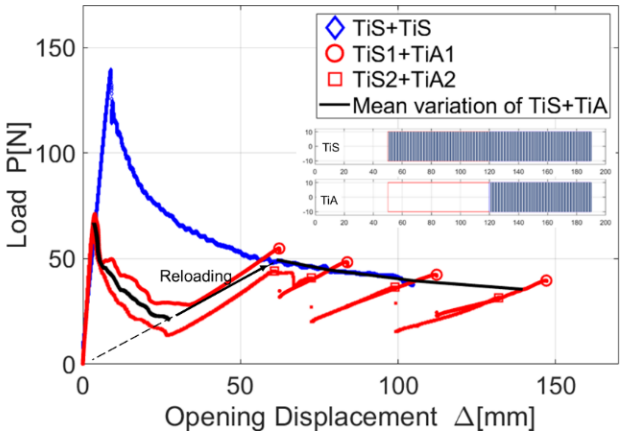

Figure 10: Variation of the opening loading in both weak and strong interfaces

The strain energy release rate curves are displayed in the figure 11. The initial segment of the curves pertains to the weak interface and is associated with a fracture energy of approximately 300 J/m². The subsequent segment of the curves corresponds to the strong interface, where the fracture energy is higher.

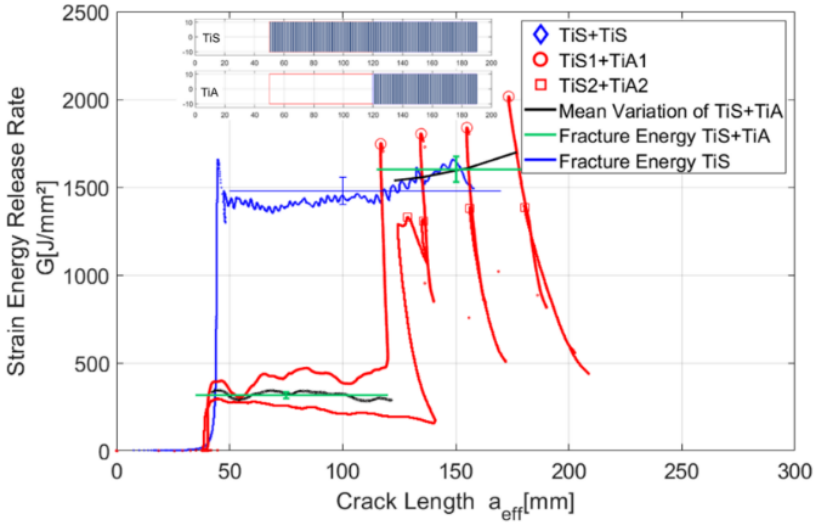

Figure 11: Strain energy release rate variation and fracture energy calculation of weak and strong interfaces for titanium alloy DCB specimens.

Here, homogenous interfaces have been characterized in aluminium and titanium alloy DCB specimens.

This section describes the successful characterization of homogeneous interfaces in DCB specimens made of both aluminium and titanium alloys. Additionally, we have created an analytical model to calculate fracture energy at crack fronts, which depends on the properties of the local interface. In the following section, we will demonstrate the experimental results and verify the accuracy of the analytical model by analysing longitudinal defects.

4.2.Longitudinal defects

DCB tests on aluminium and titanium alloys containing longitudinal heterogeneities have been carried out as explained above. The figure presented below (Figure 12) depicts how the fracture energy evolves concerning the fraction of the "weak" or "strong" zone.

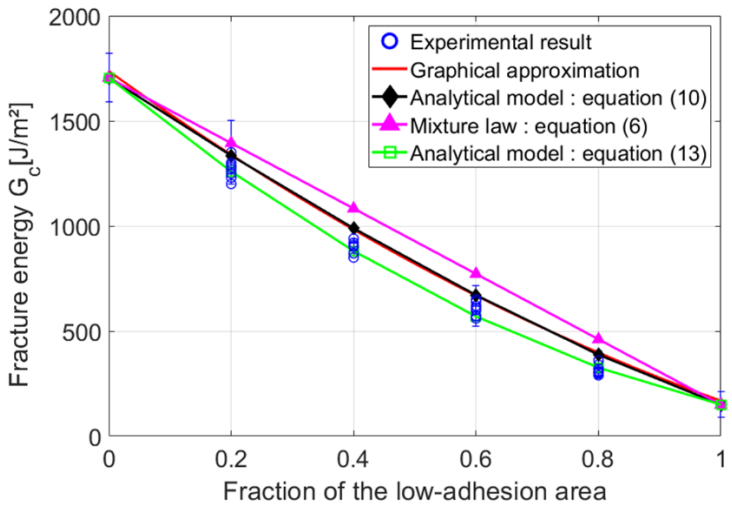

Figure 12: Fracture energy variation with low adhesion fraction in DCB specimens

We can indeed observe that this model reveals a decrease in the interface strength compared to that predicted by the simple mixture law based on energies, and it allows for the efficient calculation of the fracture energy of a heterogeneous interface. In fact, this model has shown agreement with the results obtained from experiments. The mixture law based on moments

expressed by equation 13 has demonstrated good coherence between experimental results and those estimated analytically.

The specimens are broken by initiating and then propagating a stable decohesion by performing a DCB test at a constant resulting opening speed of 2mm/min. The fracture surfaces of the specimens are presented in the figure below (see figure 13). As a reminder, the low-adhesion area is located in the middle of the specimen.

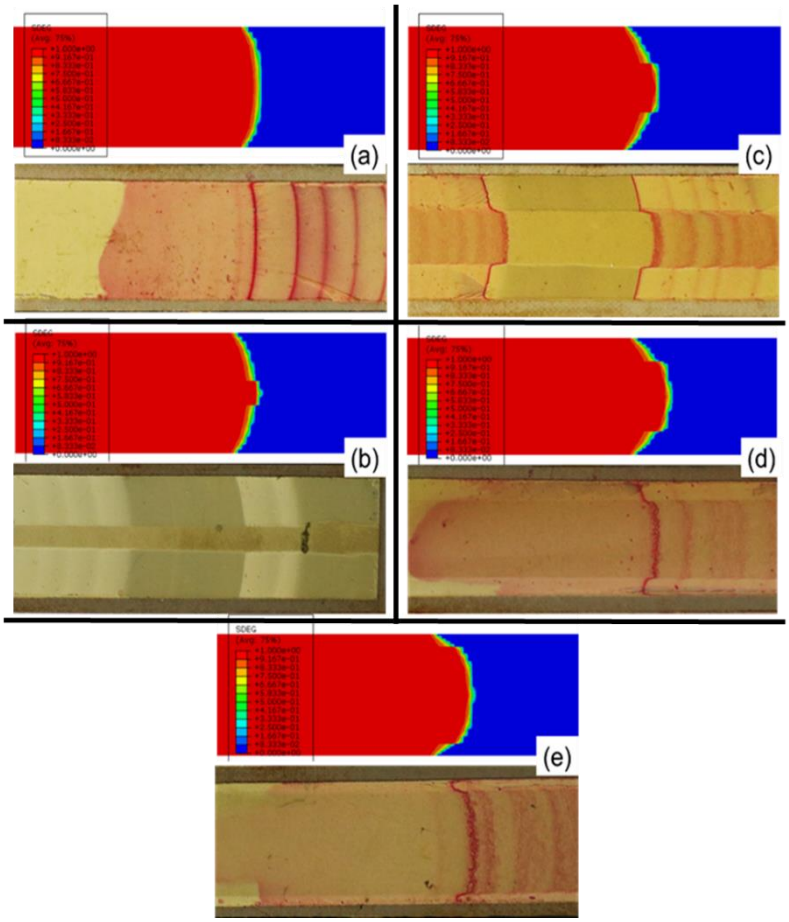

Figure 13: Comparison of Fracture Surfaces of DCB Specimens with Longitudinally Weakened Regions to Simulation Results.

(a) $f_w = 0$, (b) $f_w = 0.2$, (c) $f_w = 0.4$, (d) $f_w = 0.6$, (e) $f_w = 0.8$

The crack front changes its shape along the width of the substrate during cracking because of the heterogeneity of the material properties across the interface. The difference in material properties between the two adherents results in a non-uniform stress distribution along the

interface, which affects the propagation of the crack front. As the crack propagates, the non-uniform stress distribution leads to uneven crack front advancement, causing it to change its shape. Additionally, the heterogeneity of the material properties affects the energy release rate at the crack tip, which further influences the crack front shape.

The crack front shapes observed on the fracture surfaces of tested specimens are similar to those obtained from numerical simulations. This similarity is maintained as the crack front transitions from the strongly adhered zone to the weakly adhered zone (central part), which can be attributed to the presence of a local bending moment causing the curvature, in accordance with the law of moment mixture.

The numerical simulations depicted in figure 13, showing crack front deformation, were conducted using cohesive zone modelling, with the traction separation law employed presented in figure 14. The same figure presents also the distribution traction separation behaviour along the bonded interface in presence of longitudinal defects.

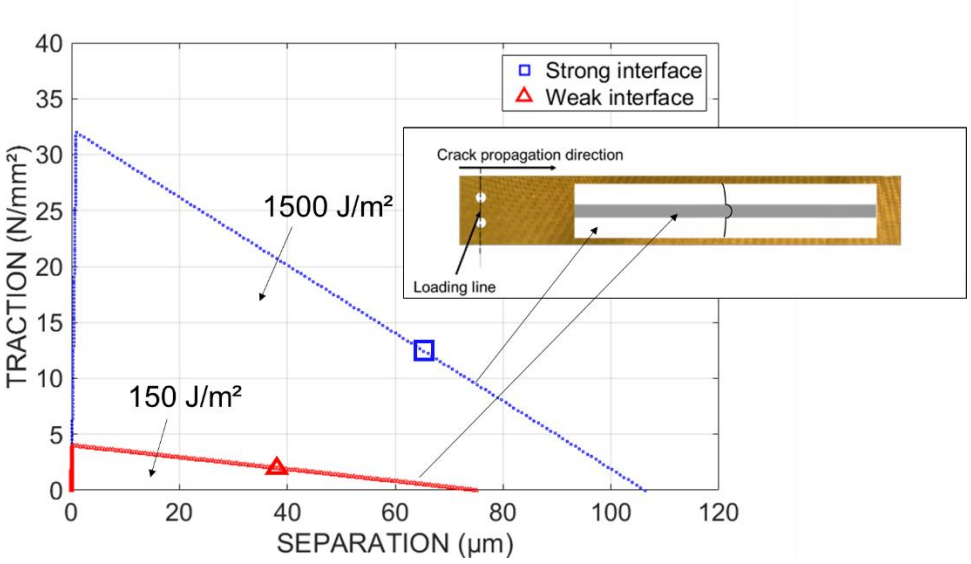

Figure 14: Traction separation laws of strong and weak interfaces of aluminium DCB substrates

The initial rigidity of cohesive laws K_w and K_s of, respectively, strong and weak interfaces are equal since the same adhesive was used ton bond substrates. K_w and K_s are calculated used equation 14.

$$K = \frac{1}{t_a}\frac{E_a(1-\vartheta)}{(1+\vartheta)(1-2\vartheta)} \tag{14}$$

Where:

E_a : Young's modulus of the adhesive equals to 2.5 GPa

ϑ : Poisson coefficient of the adhesive equals to 0.33

t_a: Adhesive thickness equals to 0.1 µm.

Cohesive law of strong and weak interfaces presented in figure 14 were tested and confronted to experimental and analytical results. The test results are presented in figure 15 and 16.

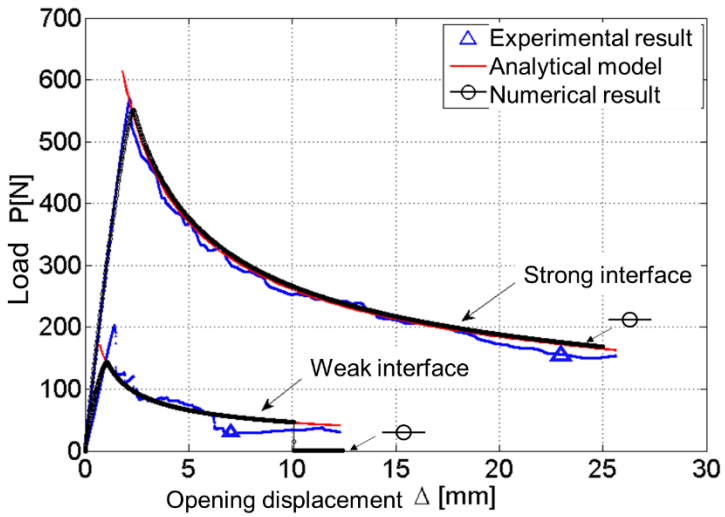

Figure 15: Simulation results using cohesive zone models for strong and weak interfaces confronted with analytical approximation and experimental tests.

In this particular case, achieving an exact replication of the experimental result is not possible due to the homogenization of the interface's global behavior enabled by the cohesive laws employed. However, it is feasible to perform a meticulous simulation by employing a local cohesive law at each energy release rate variation along the interface during crack propagation. Nevertheless, this task can be highly challenging, particularly in determining the local cohesive zone models, and executing it within Abaqus can be quite demanding.

The variation of the energy strain rate in crack front along the bonded area of the specimen has also been depicted using some other configurations on titanium alloy DCB specimens as shown above in figure 6. As a reminder, the fracture energy of a good-adhesion and low-adhesion areas has been determined in the previous section.

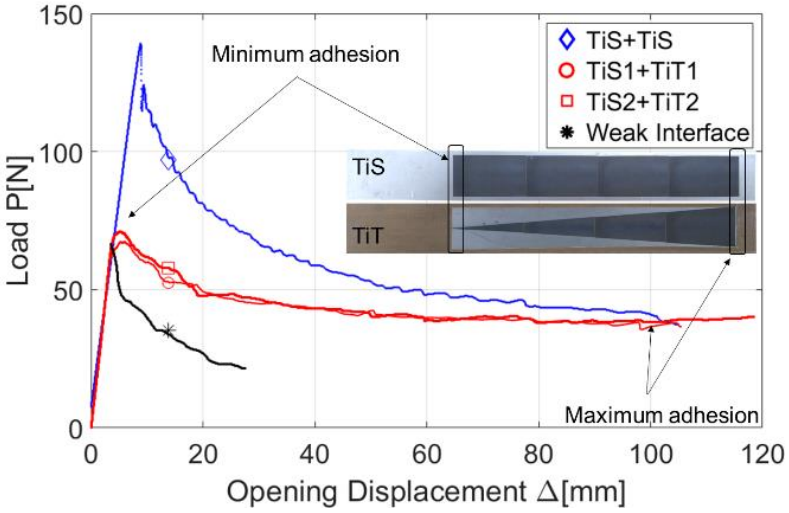

Figure 16: Mechanical behaviour of TiS+TiT Titanium alloy DCB configuration

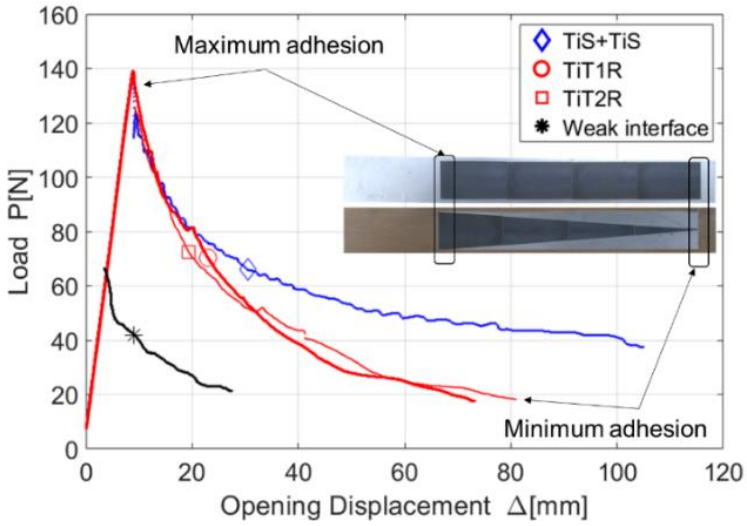

Figure 17: Mechanical behaviour of TiS+TiTR Titanium alloy DCB configuration

The region of the TiS+TiT curve where the peak occurs corresponds to the minimum level of adhesion. In this region, the TiS+TiT sample behaves in the same way as a sample with full low adhesion. As the crack propagates, the area of high adhesion gradually increases, which explains the shift towards behaviour characteristic of a zone of high adhesion. This is illustrated at the end of the curves where they meet as it can be seen in figure 17.

Moreover, when the region of strong adhesion is situated at the initial stage of crack propagation in TiTR specimens, their behaviour is comparable to that of TiS+TiT specimens. However, as the level of good adhesion diminishes, TiTR specimens exhibit a similar behaviour to that of a weak interface case.

The graphs presented below, labelled as figures 18 and 19, demonstrate how the fracture energy changes in relation to the percentage of strong adhesion surface. This analysis was conducted to enhance comprehension of the behaviour exhibited by the TiS+TiT and TiS+TiTR samples. These graphs validate the behaviour observed in figure 12, which involved conducting tests on specimens made of aluminium alloy. The fracture energy shows a curved shape that aligns with the analytical model explained by equation 13.

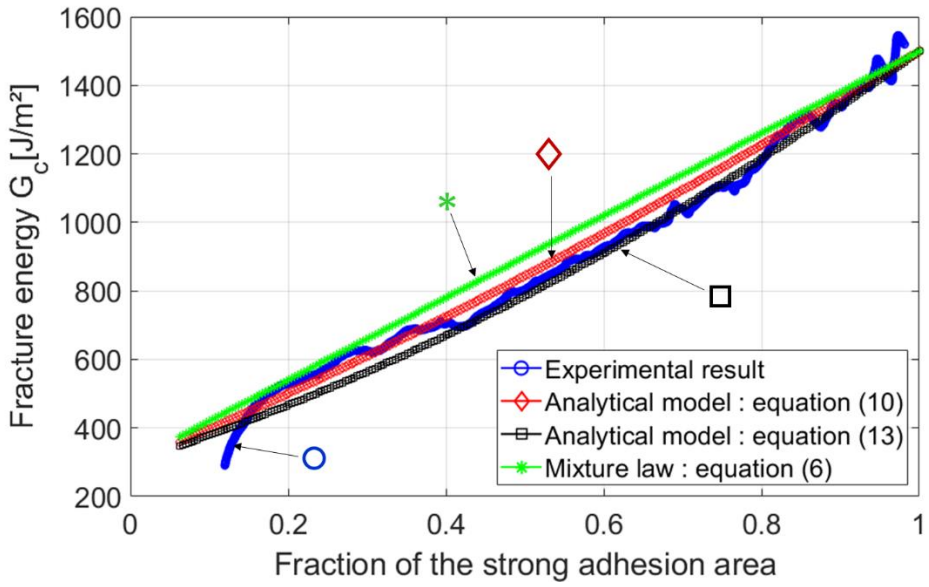

Figure 18: variation of fracture energy with strong adhesion surface

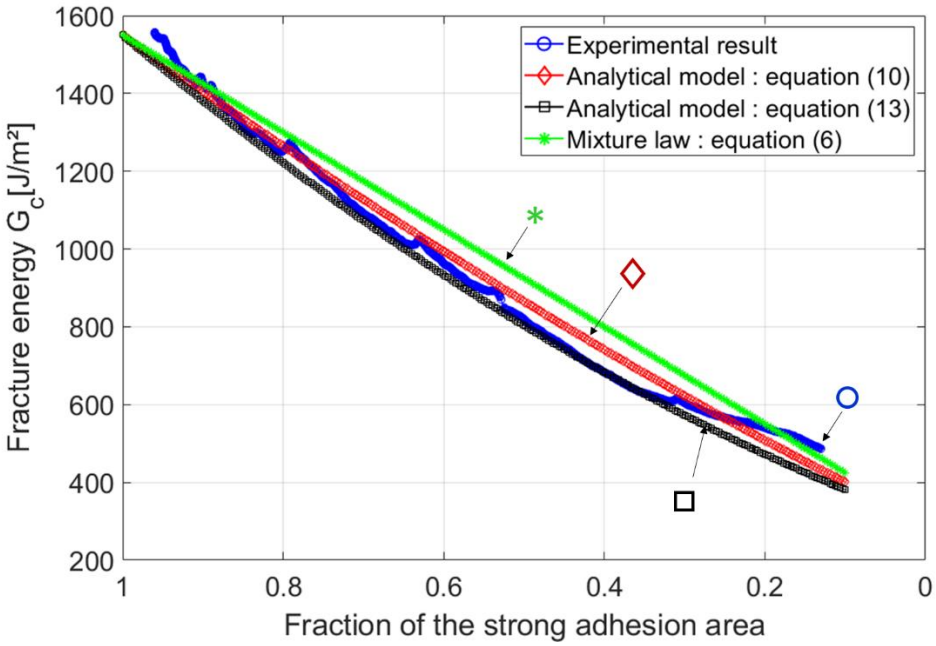

Figure 19: variation of fracture energy with strong adhesion surface

The curvature of the variation of the fracture energy as a function of the proportion of the high adhesion zone may be more significant when the adhesive is less rigid. In bonded assemblies, the effect of the Young's modulus of the adhesive on the fracture energy is that as the Young's modulus of the adhesive increases, the fracture energy also tends to increase. This is because a

stiffer adhesive can withstand greater loads before failure, which leads to higher energy absorption during fracture. Conversely, when the Young's modulus of the adhesive is lower, the adhesive is less able to resist deformation and fracture, resulting in lower fracture energy. However, it's worth noting that the relationship between Young's modulus and fracture energy is not always straightforward, as it also depends on other factors such as the geometry of the bonded interface and the magnitude of the applied load.

5. Conclusions

The study of bonding defects, whether they are related to the process, adhesive or bonding preparation, has been ongoing for a long time. Adhesion defects are those that cause adhesive ruptures that occur at the level of one of the substrate surfaces, and they are caused by poor surface preparation, contamination or degradation of the surface treatment under the effect of heat.

In this article, we focused on interface defects that are the most critical as crack propagation is faster. We were particularly interested in longitudinal defects that deform the crack front; therefore, they are responsible for a non-homogeneity of stresses during propagation. This leads to a spatial variation in fracture energy locally at the crack front. We were able too, to establish a theoretical model capable of estimating the overall fracture energy at the crack front that propagates uniformly, as it concerns longitudinal defects. The theoretical model developed was compared with experiments on DCB specimens made of aluminium and titanium alloys. A very good fit of the results was observed, which validated the experimental results obtained in this paper and previous research on the variation of fracture energy with the fraction of weak or strong adhesion.

A perspective of this work could focus on investigating the effect of adhesive stiffness and thickness on the variation of fracture energy. This will lead to the development of an analytical

model that captures the effect of a complex shape defect that better reflects reality since they are the combination of transverse (TalebAli, Jumel, & Shanahan, 2018) and longitudinal defects.

Acknowledgments

The authors would like to acknowledge the support and contribution of ALPhANOV Nouvelle-Aquitaine, France, for their assistance with the surface texturing on titanium alloys. Their expertise and technical assistance were instrumental in the success of this study.

References

Budzik, M. K., & Jensen, H. M. (2016). Experimental study of cracks at interfaces with voids. *Procedia Structural Integrity, 2*, 277 - 284.

Budzik, M., Jumel, J., & Shanahan, M. (2013). Adhesive fracture of heterogeneous interfaces. *Philosophical magazine, 93*(19), 2413 - 2427.

Chan, E., Ahn, D., & Crosby, A. (2007). Adhesion of patterned reactive interfaces. *The journal of adhesion, 83*, 473 - 489.

Cuminatto, C., Parry, G., & Braccini, M. (2015). A model for patterned interfaces debonding - Application to adhesion tests. *International journal of solids and structures, 75 - 76*, 122 - 133.

Jorgensen, S. H., & Budzik, M. (2017). Crack growth along heterogeneous interface during the DCB experiment. *International journal of solids and structures, 120*, 278 - 291.

Jumel, J. (2017). Crack propagation along interface having randomly fluctuating mechanical properties during DCB test finite difference implementation - Evaluation of Gc distribution with effective crack length technique. *Composites part B : Engineering, 116*, 253 - 265.

Karachalios, E., Adams, R., & DaSilva, L. (2013). Strength of single lap joints with artificial defects. *International journal of adhesion and adhesives, 45*, 69 - 76.

Litteken, C., & Dauskardt, R. (2003). Adhesion of polymer thin-films and patterned lines. *International journal of fracture, 120*(1), 475 - 485.

Loumena, C., Cherif, M., Taleb Ali, M. J., & Kling, R. (2017). Laser surface preparation for adhesive improvement of Ti6A14V. *Proceeding of SPIE, Laser-based Micro and Nanoprocessing XI.*

Ranade, S. (2014). *Performance evaluation and durability studies of adhesives bonds.* Virginia: Polytechnic Institute and State University.

Ranade, S., Guan, Y., Moore, R., Dillard, J., Batra, R., & Dillard, D. (2018). Characterizing fracture performance and the interaction of propagating. *International journal of adhesion and adhesives, 82*, 196 - 205.

Scotch-Weld, 3. (2009). *Structural adhesive film AF191, Technical datasheet.*

Tadepalli, R., Turner, K. T., & Thompson, C. V. (2008). Effects of patterning on the interface toughness of wafer-level Cu-Cu bonds. *Acta Materialia, 56*(3), 438 - 447.

Taleb Ali, M. (2018). *Effets des défauts d'adhésion sur la résistance mécanique des assemblages collés.* Talence: I2M, Bordeaux University.

TalebAli, M., Jumel, J., & Shanahan, M. (2018). Effect of adhesion defects on crack propagation in double cantilever beam test. *International journal of adhesion and adhesives, 84*, 420 - 430.